

# Automatic Method for Assessment of Telangiectasia Degreeing by Mathematical Morphology

FRANKLIN CÉSAR FLORES<sup>1</sup>, ROBERTO DE ALENCAR LOTUFO<sup>1</sup>,  
STELA ISERNHAGEN<sup>1</sup>, LEONARDO MARQUES ROCHA<sup>1</sup>  
ALEXANDRE GONÇALVES SILVA<sup>1</sup> AND EDUARDO FACCINI ROCHA<sup>2</sup>

<sup>1</sup> Faculdade de Engenharia Elétrica e Computação - UNICAMP  
P.O.Box 6101 13083-970  
Campinas, SP - Brazil

<sup>2</sup> Faculdade de Ciências Médicas - UNICAMP  
P.O.Box 6111 13083-970  
Campinas, SP - Brazil  
{fcflores,lotufo}@dca.fee.unicamp.br

**Abstract.** This paper presents an automatic method to assess telangiectasia degreeing, by estimating the reduction of the varicose area from pre to post-treatment using digital image analysis techniques. First both images are geometrically transformed and color space reduced, in order to make them suitable for processing. Next, the varicose veins are segmented via watershed transform and the varicose areas in both images are detected. Finally, the assessment degreeing is done. The method was applied to twenty patients and the results were very consistent, according to the analysis of six vascular specialists.

## 1 Introduction

Telangiectasias [13, 16, 5, 17] are superficial vases visible by the human eye. These vases represent intradermics dilated veins. They are also known as microvaricose veins.

Some telangiectasias are treated by sclerotherapy [16, 5, 17] and in some of them the clearing degree of the telangiectasias are assessed by photo analysis. This assessment is usually done by vascular specialists. Digital photos have been showed themselves helpful in dermatologic assessments [4, 3].

Another sclerotherapy method with assessed results by photo analysis is proposed by [13]. The digital photos of pre and post-treatment were standardized as to their distance, light exposure, aperture time and covered a 49 square centimeters area assigned by four ink dots, which remained throughout the analysis period. Assessments were done to twenty patients. The initial and final digital photos were judged by six observers, according to the clearing degree of the telangiectasias. Their judgements were compared to the degreeing supplied by the automatic technique described in this work.

This paper is focused on the description of an automatic method to assess telangiectasia degreeing, by analyzing the reduction of the varicose area from the pre-treatment photo to the post-treatment one.

First both images (pre and post-treatment) are transformed, geometrical and radiometrically, in order to make them suitable for processing. Next, the varicose areas are detected through segmentation of the varicose veins. Finally, the reduction of the varicose area between the photos is computed. The automatic assessment is given by the analysis of the reduction computed by the method.

A main difficulty of the automatic varicose vein detection is that there is no contrast reference between the skin and the varicose veins. Some methods as the histogram analysis and automatic detection of threshold values were not robust when applied to the images. The best robustness was achieved with the application of the watershed from markers [11, 2] technique, that segments the varicose veins from markers selected by a contrast parameter  $p$ .

This paper is organized as follows. Section 2 presents some definitions of the techniques used in our approach. Section 3 introduces the method to automatic assessment of telangiectasia degreeing, detailing its three steps. Section 4 shows some experimental results. Finally, we conclude this work with some discussion in Section 5.

## 2 Preliminary Definitions

Let  $E \subset \mathbb{Z} \times \mathbb{Z}$  be a rectangular finite subset of points. Let  $K = [0, k]$  be a totally ordered set. Denote by  $Fun[E, K]$  the set of all functions  $f : E \rightarrow K$ . An *image* is one of these functions (called graylevel functions). Particularly, if  $K = [0, 1]$ ,  $f$  is a binary image. An *image operator* (*operator*, for simplicity) is a mapping  $\psi : Fun[E, K] \rightarrow Fun[E, K]$ .

Let  $L = K \times K \times K$ . A color image is a function  $f : E \rightarrow L$ , and the set of all color images is denoted by  $Fun[E, L]$ .

Let  $N(x)$  be the set containing the *neighborhood*  $[9, 6]$  of  $x$ ,  $x \in E$ . We define a *path* from  $x$  to  $y$ ,  $x, y \in E$  as a sequence  $C = (p_0, p_1, \dots, p_n)$  from  $E$ , where  $p_0 = x$ ,  $p_n = y$  and  $\forall i \in [0, n-1], p_i \in N(p_{i+1})$ .

A *connected subset* of  $E$  is a subset  $X \subset E$  such that,  $\forall x, y \in X$ , there is a path  $C$  entirely inside  $X$ .

Let  $f \in Fun[E, K]$ . A *flat zone* of  $f$  is a connected subset  $X \subset E$ , such that  $f(x) = f(y)$ ,  $\forall x, y \in X$ .

### 2.1 Some Morphological Operators

The *opening top-hat* and *closing top-hat* operators are given respectively by,  $\forall f \in Fun[E, K]$ ,

$$th_{\neg\gamma_B}(f) = f - \gamma_B(f)$$

and

$$th_{\phi_B}(f) = \phi_B(f) - f,$$

where  $B \subset E$  is the *structuring element* and  $\gamma_B$  and  $\phi_B$  are, respectively, the morphological opening and the morphological closing [14, 8].

The *inf-reconstruction* operator is given by,  $\forall f, g \in Fun[E, K]$ ,

$$\rho_{B,g}(f) = \delta_{B,f}^{\infty}(g)$$

where  $B \subset E$  is the structuring element,  $n \in \mathbb{Z}_+$  and  $\delta_{B,f}^n$  is the *n-conditional dilation* operator [14, 8].  $\delta_{B,f}^{\infty}(g)$  means that the dilation is applied till idempotency.

Let  $\mathcal{B}$  be the set of all flat zones valued 1 in a binary image. Let  $a \in \mathbb{Z}_+$  be an area threshold. Let  $\mathcal{B}_a \subset \mathcal{B}$  be the set of all flat zones  $F \in \mathcal{B}$  whose area is greater than  $a$ . The *area opening* operator is given by,

$$\gamma_a^{\text{area}}(f) = \bigvee_{F \in \mathcal{B}_a} \gamma_F(f).$$

The dual operator of area opening is the *area closing*. This filter is a mapping  $\phi_a^{\text{area}}$ , given by,

$$\phi_a^{\text{area}}(f) = \nu(\gamma_a^{\text{area}}(\nu(f))).$$

where  $\nu(f) = k - f$ , is the negation of  $f$ .

### 2.2 Geometric Deformation via Binding Points

In order to register the images in our approach, we use geometrical transformation via binding points [10, 7]. The coefficients required to transform the images are computed given four pairs of corresponding points in the original image and in the deformed one. These points define eight bilinear equations solved by the Gauss method, and they provide the transformation coefficients.

Usually, given an image  $f \in Fun[E, K]$ , the deformed image  $g \in Fun[E, K]$  can be computed as follows,  $\forall (x, y) \in E$ :

$$g(\hat{x}, \hat{y}) = f(x, y) : \begin{cases} \hat{x} = c_1x + c_2y + c_3xy + c_4 \\ \hat{y} = c_5x + c_6y + c_7xy + c_8 \end{cases}$$

The mapping defined above can, since  $E \subset \mathbb{Z} \times \mathbb{Z}$ , estimate non-existent coordinates by rounding the results of  $\hat{x}$  and  $\hat{y}$ . It can be avoided by computing the inverse transformations, given by,

$$f(x, y) = g(\hat{x}, \hat{y}) : \begin{cases} x = c_1\hat{x} + c_2\hat{y} + c_3\hat{x}\hat{y} + c_4 \\ y = c_5\hat{x} + c_6\hat{y} + c_7\hat{x}\hat{y} + c_8 \end{cases}$$

where the points in the original image are mapped given the position of points in the deformed image. The binding points make it possible since they define the areas where the corresponding points are mapped.

Section 3.1.1 presents how the binding points are automatically detected in the proposed method.

## 3 The Proposed Technique

This section describes the method applied to quantitative analysis of sclerotherapy results. It receives as input a pair of images: one of them is a digital photo of the varicose area, delimited by four point ink dots, taken before the treatment; the other one is a photo of the same area, taken after the treatment. As output, the method gives the degreering rate of varicose veins, achieved by the sclerotherapy.

Let  $a \in Fun[E, L]$  and  $b \in Fun[E, L]$  be, respectively, the pre-treatment and post-treatment input images. The proposed method is divided in three steps: registration and color transformation, varicose veins segmentation, and computation of the degreering rate.

### 3.1 Registration and Color Transformation

In this first step, the input images are transformed in order to show only the varicose region. The output images  $a_{reg} \in Fun[E, K]$  and  $b_{reg} \in Fun[E, K]$  have the same size of  $a$  and  $b$  and show only the area delimited by the four ink dots. The images are obtained by an image registration, by application of a geometrical

transformation [10, 7], and by a color transformation to gray scale.

### 3.1.1 Automatic Detection of Binding Points

To apply the geometrical deformation via binding points to  $a$ , we must, a priori, define these binding points. Once we want to have an image containing just the varicose area, we must bind the points in the center of the ink dots to their respective points in the output image, located in the image corners. The center of the upper left ink dot must be bound to the upper left corner in the output image, and so on.

The binding points in the input image are found as follows:

The luminance of the color image  $a$  is computed and stored in a gray scale image. Let  $a_{gray} \in Fun[E, K]$  be such image. In the next, the following operator is applied and the ink dots are segmented.

$$\psi_{inkdot}(a_{gray}) = \Phi_{B_c}(\gamma_{30}^{area}(\tau_{30}(th_{\phi_{B_{disk}}}(a_{gray})))),$$

where  $B_{disk}$  is a disk structuring element with radius 7,  $B_c$  is a elementary cross structuring element,  $\tau_n$  is a threshold function which selects gray levels greater than or equal to  $n$ , and  $\Phi_{B_c}$  is the closing holes operator [1].

Since the size of the images does not vary and the ink dots are well defined despite the contrast variation, the  $\psi_{inkdot}$  operator is robust. The result of this operator is a binary image containing the four ink dots. The next steps consists of computing the centroid of each ink dot.

Once these points are bound, the geometric transformation is done. The color image  $a_{aff} \in Fun[E, L]$ , which shows only the varicose area, is the result of this process.

Figure 1 (a) shows a pre-treatment image. Figure 1 (b) shows the ink points detected. Figure 1 (c) shows the deformation via binding points.

### 3.1.2 Color Transformation

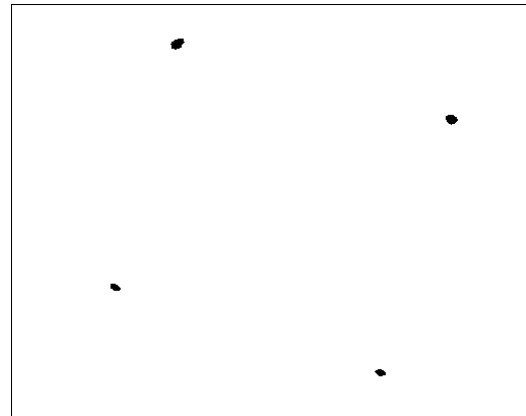
Once  $a_{aff}$  is computed, a color transformation is done in order to simplify the registered image to an gray scale one, with the varicose veins enhanced. Let  $a_r, a_g \in Fun[E, K]$ , be, respectively, the red and green informations of  $a_{aff}$ . The gray scale image  $a_{reg} \in Fun[E, K]$  is given by,

$$a_{reg} = (a_r - a_g) + \nu(a_r).$$

$a_{reg}$  is the result of the first step of the proposed method. Since the varicose veins present reddish tones, the given transformation not only transforms the color image to a gray level one, but also enhances the veins.



(a)



(b)



(c)

Figure 1: (a) Original Image (b) Ink Points Detected (Image Negated) (c) Geometric Transformation

The image shows only the varicose veins and the color transformation enhanced these veins. The enhancement of the veins is achieved The first step of the proposed method is done with both images,  $a$  and  $b$  (and let us denote by  $b_{reg}$  the image  $b$  transformed). Figure 2 shows Fig. 1 (c) with the enhanced veins after the color transformation.

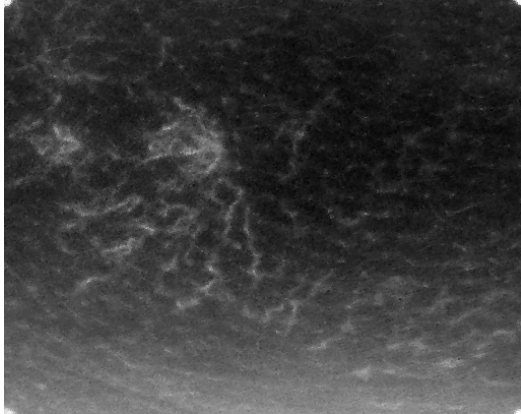


Figure 2: Color Transformation

### 3.2 Varicose Veins Segmentation

After the registration and color transformation of  $a$  and  $b$ , the segmentation of the varicose veins is done in  $a_{reg}$  and  $b_{reg}$ .

First, it is applied an opening top-hat, followed by application of a alternated sequential filter by reconstruction [8, 14]. The first operator is applied to regularize the the image background and to enhance even more the varicose veins. The second operator is a smooth filtering of the top-hat result. Let  $a_{reg}$  be the resulting image from the previous step, the composition of these operators defines an operator  $\zeta_1 : Fun[E, K] \rightarrow Fun[E, K]$ , given by,

$$\zeta_1(a_{reg}) = \gamma\phi_{1,B,B_c}(th_{\neg\gamma B_{disk}}(a_{reg})),$$

where  $B_{disk}$  is a disk structuring element with radius 5 and  $\gamma\phi_{n,B,B_c} : Fun[E, K] \rightarrow Fun[E, K]$  is the alternating sequential filter by reconstruction. Figure 3 presents the result of  $\zeta_1$  applied to Fig. 2. The image was negated for best viewing.

In the following, it is computed the internal borders of  $\zeta_1(a_{reg})$ , through application of gradient operator. It its done in order to apply the watershed with markers technique [11, 2, 9]. The operator  $\zeta_2 : Fun[E, K] \rightarrow Fun[E, K]$  is given by,

$$\zeta_2 = \zeta_1(\cdot) - \varepsilon_B(\zeta_1(\cdot)),$$



Figure 3: Veins Enhanced (Image Negated)

where  $B$  is the elementary cross structuring element and  $\zeta_1(\cdot)$  is the result of application of the  $\zeta_1$  operator. Figure 4 shows the internal borders of Fig. 3 detected. Again, the image was negated for a best viewing.

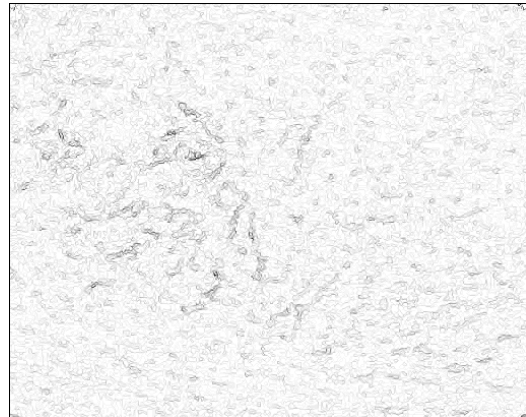


Figure 4: Morphological Gradient (Image Negated)

Let  $p \in K$  be the contrast parameter which defines the varicose veins to be segmented. The markers are computed by taking all regional minima with contrast greater than or equal to  $p$ . Let  $\zeta_3 : Fun[E, K] \rightarrow Fun[E, K]$  be the operator that computes this set of markers when applied to  $\zeta_2(\cdot)$ . Figure 5 shows the application of  $\zeta_3$  to Fig. 4 and the marker detection for a contrast parameter  $p = 3$ . Section 4 presents some experimental results using  $p = 2$  and  $p = 3$ .

Once the internal borders of the enhanced veins were computed and markers were imposed, the watershed with markers technique can be applied to segment the veins. Let  $\zeta_4 : Fun[E, K] \rightarrow Fun[E, K]$  be the application of the watershed operator [12, 15] to

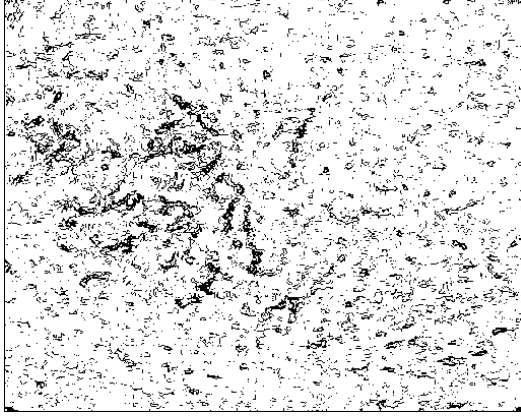


Figure 5: Markers Imposed Using Contrast Parameter  $p = 3$

$\zeta_2(\cdot)$  using  $\zeta_3(\cdot)$  as the set of markers.  $\zeta_4(\cdot)$  is a binary image containing the watershed lines to the varicose veins. The watershed results is shown in Fig. 6.

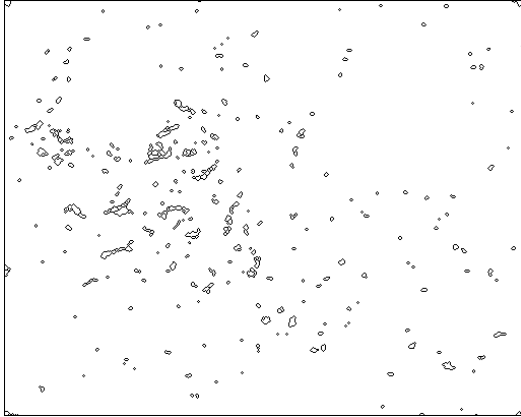


Figure 6: Watershed Lines (Image Negated)

Following the application of watershed with markers, the regions delimited by the watershed lines, whose area is lower than or equal to 100, are filled. It is done in order to detect the area occupied by the varicose veins. However, it is also necessary to erase the watershed lines delimiting regions whose area were not filled. It is done by a connected filtering. The operator  $\zeta_5 : Fun[E, K] \rightarrow Fun[E, K]$  which fills the delimited regions with area lower than or equal to 100 and erases the remaining watershed lines is given by

$$\zeta_5 = \gamma_{15}^{\text{area}} \phi_{100}^{\text{area}}.$$

Figure 7 shows the application of  $\zeta_5$  to Fig. 6. Note the filling of the most delimited areas and the elimination of the remaining watershed lines.



Figure 7: Closing of Selected Areas and Filtering of Remaining Lines (Image Negated)

Finally, it is applied an operator to remove the ink dots from the corners of the image, since they eventually are segmented with the varicose veins. The ink dots are removed by inf-reconstructing them and removing them by subtraction. Let  $frm \in Fun[E, K]$  be the frame function [1] with dimensions equals  $\zeta_5(\cdot)$ . The operator  $\zeta_6 : Fun[E, K] \rightarrow Fun[E, K]$ , given by,

$$\zeta_6 = \rho_{B, \zeta_5(\cdot)}(frm),$$

(where  $B$  is the structuring element) is the last one applied in the second part of the method proposed in this paper and provides a binary image which blobs represent the area where the varicose veins appear in the image. Figure 8, with the ink points removed, are ready for assessment in the last step of the methodology.

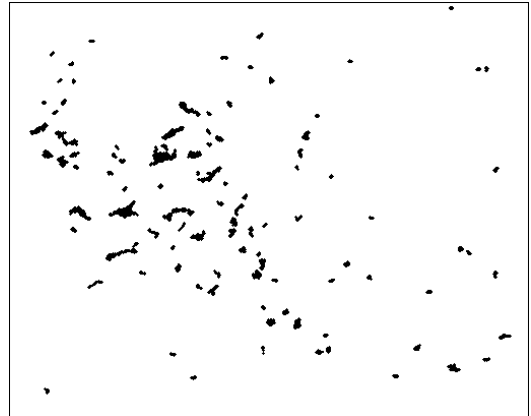


Figure 8: Ink Points Removal (Image Negated)

Let  $\Omega : Fun[E, K] \rightarrow Fun[E, K]$  be the operator defined by the concatenation of the  $\zeta_i$  operators. Since

$a_{reg}$  and  $b_{reg}$  are the results of the first step of the proposed method, it is necessary to apply  $\Omega(a_{reg})$  and  $\Omega(b_{reg})$  in order to compute the degreering rate in the third and last step of the methodology.

### 3.3 Computation of the Degreering Rate

Let  $n$  be the number of pixels valued 1 in the image. The degreering rate  $r : Fun[E, K] \times Fun[E, K] \rightarrow \mathbb{R}$  of varicose veins from  $a$  to  $b$  is given by,

$$r(a_{reg}, b_{reg}) = 1 - \frac{n(\Omega(b_{reg}))}{n(\Omega(a_{reg}))}.$$

The closer the value of  $r$  is to 1, the greater is the reduction of the varicose veins.

## 4 Experimental Results

The experiments were done using a set of digital photos taken from twenty patients (twenty-three areas). It was taken from each patient three photos: the first one was taken before the sclerotherapy is done. The second photo was also taken before the sclerotherapy and it was taken a few days later. The last photo was taken after the sclerotherapy. Let us call them, respectively,  $a$ ,  $b$  and  $c$ .

For each patient, the degreering rate was computed from  $a$  to  $b$ , from  $a$  to  $c$  and from  $b$  to  $c$ . It was expected that  $r(a_{reg}, b_{reg}) \approx 0$  and  $r(a_{reg}, c_{reg}) \approx r(b_{reg}, c_{reg})$ .

Two set of experiments were done, each of them using a different contrast parameter  $p$ . Table 1 shows the degreering rate computed using  $p = 2$ . Table 2 shows the degreering rate computed using  $p = 3$ . The first column of both Tables is a code for each patient.

Note that, when the results of  $r(a_{reg}, b_{reg})$  are not close to 0, the results of  $r(b_{reg}, c_{reg})$  and  $r(a_{reg}, c_{reg})$  are not reliable (they are not even approximated).

Figure 9 presents three registered images, taken from patient 13015. The first two images were taken before the treatment and the last one was taken after the treatment. Figure 10 shows the segmentation of varicose veins of each image of Fig. 9.

The degreering rates computed by the proposed method were presented to six specialists in sclerotherapy. The statistical analysis concludes that the rates achieved by the proposed automatic method are consistent. The complete assessment done by the specialists and the comparison with the computer performance can be found in [13].

The degreering rates computed by the proposed method were compared to the assessment done by six specialists in sclerotherapy. The results were statistically analyzed and it was concluded that the rates

Patient	$r(a_{reg}, b_{reg})$	$r(b_{reg}, c_{reg})$	$r(a_{reg}, c_{reg})$
12413	0.29	0.59	0.42
12504	0.22	-0.32	-0.70
12623a	-0.40	0.58	0.70
12623b	0.06	0.71	0.69
12640	0.09	0.77	0.75
12667	0.01	0.52	0.52
12668	0.19	0.64	0.55
12672	0.20	0.74	0.67
12700	-0.25	-1.13	-0.70
12709	0.22	0.54	0.41
12710	0.13	0.06	-0.08
12713	-0.32	0.48	0.61
12715	-0.07	0.66	0.68
12721a	-0.27	-0.09	0.14
12721b	-0.10	0.33	0.40
12726	-0.13	0.64	0.68
12808	0.02	0.66	0.65
12904	0.13	0.11	-0.02
12931a	0.01	0.40	0.40
12931b	-0.01	0.48	0.48
12932	-0.13	0.38	0.45
13015	0.33	0.21	-0.19
13057	-0.08	0.69	0.71

Table 1: Automatic Assessment of Degreering Rate of Varicose Veins - Using Contrast Parameter  $p = 2$ .

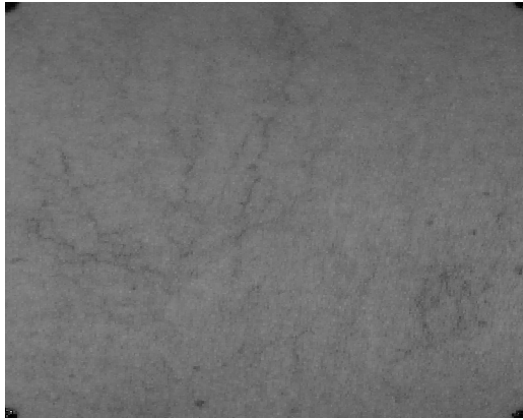
achieved by the proposed automatic method are consistent. The complete assessment done by the specialists and the comparison with the computer performance can be found in [13].

## 5 Conclusion

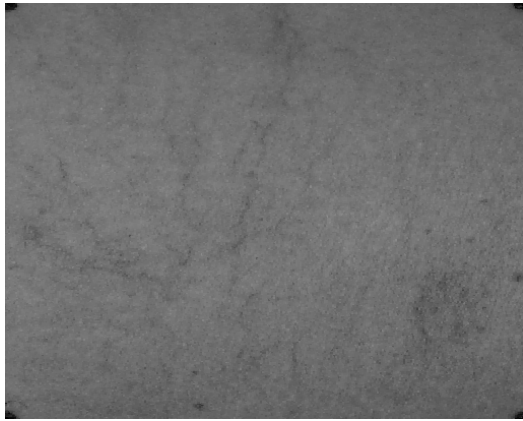
This paper presents an automatic method applied to assessment of telangiectasia degreering achieved by lower-limb sclerotherapy. The doctor delimits the area where the treatment is done with four ink points and digital photos are taken from this area, before and after the sclerotherapy. The method proposed in this paper is applied and the degreering rate is computed from pre to post-treatment.

The method was applied to a set of digital photos taken from various patients and the results were quite satisfactory, since the specialists stated that the assessment done by our approach was consistent.

The techniques used in the first step of the proposed method showed robustness, both in the registration and in the color transformation. Among the techniques explored, the top-hat and watershed with markers showed themselves accurate to avoid the prob-



(a)

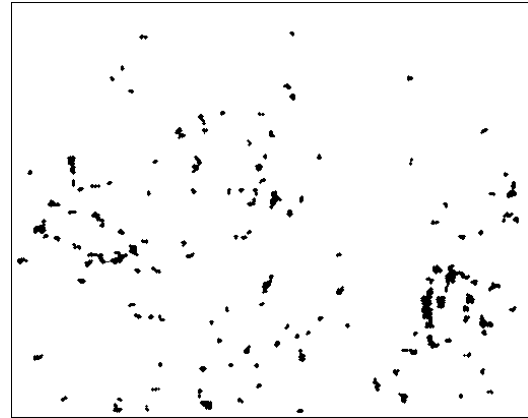


(b)

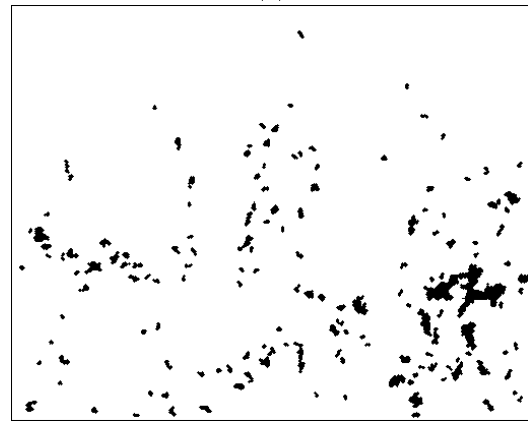


(c)

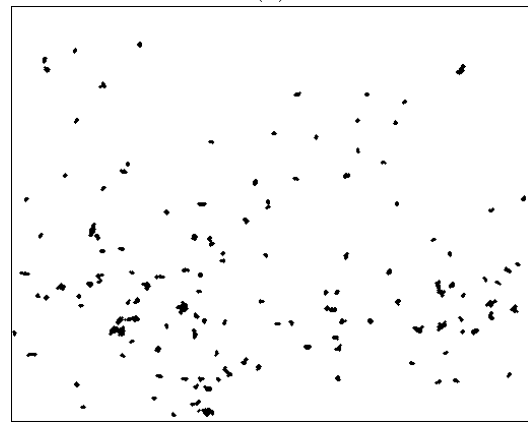
Figure 9: Patient 13015 (a) First Pre-Treatment Image (b) Second Pre-Treatment Image (c) Post-Treatment Image



(a)



(b)



(c)

Figure 10: Patient 13015 (a) Segmentation of the First Pre-Treatment Image (b) Segmentation of the Second Pre-Treatment Image (c) Segmentation of the Post-Treatment Image

Patient	$r(a_{reg}, b_{reg})$	$r(b_{reg}, c_{reg})$	$r(a_{reg}, c_{reg})$
12413	0.12	0.65	0.60
12504	0.24	0.30	0.07
12623a	-0.16	0.87	0.89
12623b	0.07	0.82	0.81
12640	0.27	0.89	0.85
12667	0.08	0.65	0.62
12668	0.03	0.84	0.83
12672	0.12	0.69	0.64
12700	-0.45	-0.69	0.17
12709	0.34	0.85	0.77
12710	0.04	0.45	0.43
12713	-0.14	0.67	0.71
12715	-0.65	0.52	0.71
12721a	-0.10	0.45	0.50
12721b	-0.16	0.66	0.71
12726	0.01	0.83	0.83
12808	0.05	0.84	0.83
12904	0.50	0.35	-0.31
12931a	0.08	0.69	0.67
12931b	-0.05	0.67	0.69
12932	-0.07	0.69	0.70
13015	0.33	0.48	0.23
13057	0.11	0.92	0.91

Table 2: Automatic Assessment of Degreeing Rate of Varicose Veins - Using Contrast Parameter  $p = 3$ .

lem of lack of contrast between varicose veins and skin.

## References

- [1] J. Barrera, G. J. F. Banon, R. A. Lotufo, and R. Hirata Jr. MMach: a Mathematical Morphology Toolbox for the Khoros System. *Electronic Imaging*, 7(1):174–210, 1998.
- [2] S. Beucher and F. Meyer. *Mathematical Morphology in Image Processing*, chapter 12. The Morphological Approach to Segmentation: The Watershed Transformation, pages 433–481. Marcel Dekker, 1992.
- [3] A. Bittorf et al. Resolutions Requirements for Digital Images in Dermatology. *J. Am. Acad. Dermatol.*, 37:195–198, 1997.
- [4] J.C. Kvedar et al. The Substitution of Digital Images for Dermatologic Physical Examination. *Arch. Dermatol.*, 133:161–167, 1997.
- [5] E.F. Bernstein et alli. Treatment of Spider Veins with the 595nm Pulsed-Dye Laser. *J. Am. Acad. Dermatol.*, 39:746–750, 1998.
- [6] F. C. Flores. Segmentação de Sequências de Imagens por Morfologia Matemática. Dissertação de Mestrado, Instituto de Matemática e Estatística - Universidade de São Paulo, Outubro 2000.
- [7] R. C. Gonzalez and R. E. Woods. *Digital Image Processing*. Addison-Wesley Publishing Company, 1992.
- [8] H. J. A. M. Heijmans. *Morphological Image Operators*. Academic Press, Boston, 1994.
- [9] R. Hirata Jr. Segmentação de Imagens por Morfologia Matemática. Dissertação de Mestrado, Instituto de Matemática e Estatística - USP, março 1997.
- [10] S.K. Feiner J. Foley, A. vanDam and J.F. Hughes. *Computer Graphics - Principles and Practice*. Addison-Wesley Publishing Company, 2nd edition, 1990.
- [11] F. Meyer and S. Beucher. Morphological Segmentation. *Journal of Visual Communication and Image Representation*, 1(1):21–46, September 1990.
- [12] R. A. Lotufo and A. X. Falcão. The Ordered Queue and the Optimality of the Watershed Approaches. In J. Goutsias, L. Vincent, and D. S. Bloomberg, editors, *Mathematical Morphology and its Applications to Image and Signal Processing*, volume 18, pages 341–350. Kluwer Academic Publishers, 2000. Fifth ISMM.
- [13] E. F. Rocha. Análise Quantitativa dos Resultados de Escleroterapia com o Uso de Fotografia Digital e um Programa de Computador. Dissertação de Mestrado, FCM - UNICAMP, Dezembro 2001.
- [14] J. Serra. *Image Analysis and Mathematical Morphology*. Academic Press, 1982.
- [15] L. Vincent and P. Soille. Watersheds in Digital Spaces: An Efficient Algorithm Based on Immersion Simulations. *IEEE Transactions on Pattern Analysis and Machine Intelligence*, 13(6):583–598, June 1991.
- [16] R.A. Weiss and N. Sadick. Epidermal Cooling Crystal Collar Device for Improved Results and Reduced Side Effects on Leg Telangiectasias Using Intense Pulsed Light. *Dermatol. Surg.*, 26:1015–1018, 2000.
- [17] R.A. Weiss and M.A. Weiss. *Handbook of Venous Disorders*, chapter Sclerotherapy of Telangiectasia, pages 355–373. Chapman and Hall Medical, 1996.